*Protein Science* (1999), *8*:307–317. Cambridge University Press. Printed in the USA.


# Comparison of the backbone dynamics of the apo- and holo-carboxy-terminal domain of the biotin carboxyl carrier subunit of *Escherichia coli* acetyl-CoA carboxylase

XIANG YAO,[1,2] CYLBURN SODEN, JR.,[1,2] MICHAEL F. SUMMERS,[1,2] AND DOROTHY BECKETT[1]

[1]Department of Chemistry and Biochemistry, University of Maryland Baltimore County, 1000 Hilltop Circle, Baltimore, Maryland 21250
[2]Howard Hughes Medical Institute, University of Maryland Baltimore County, 1000 Hilltop Circle, Baltimore, Maryland 21250

(RECEIVED July 29, 1998; ACCEPTED October 26, 1998)

**Abstract**

The biotin carboxyl carrier protein (BCCP) is a subunit of acetyl-CoA carboxylase, a biotin-dependent enzyme that catalyzes the first committed step of fatty acid biosynthesis. In its functional cycle, this protein engages in heterologous protein–protein interactions with three distinct partners, depending on its state of post-translational modification. Apo-BCCP interacts specifically with the biotin holoenzyme synthetase, BirA, which results in the post-translational attachment of biotin to a single lysine residue on BCCP. Holo-BCCP then interacts with the biotin carboxylase subunit of acetyl-CoA carboxylase, which leads to the addition of the carboxylate group of bicarbonate to biotin. Finally, the carboxy-biotinylated form of BCCP interacts with transcarboxylase in the transfer of the carboxylate to acetyl-CoA to form malonyl-CoA. The determinants of protein–protein interaction specificity in this system are unknown. The NMR solution structure of the unbiotinylated form of an 87 residue C-terminal domain fragment (residue 70–156) of BCCP (holoBCCP87) and the crystal structure of the biotinylated form of a C-terminal fragment (residue 77–156) of BCCP from *Escherichia coli* acetyl-CoA carboxylase have previously been determined. Comparative analysis of these structures provided evidence for small, localized conformational changes in the biotin-binding region upon biotinylation of the protein. These structural changes may be important for regulating specific protein–protein interactions. Since the dynamic properties of proteins are correlated with local structural environments, we have determined the relaxation parameters of the backbone $^{15}N$ nuclear spins of holoBCCP87, and compared these with the data obtained for the apo protein. The results indicate that upon biotinylation, the inherent mobility of the biotin-binding region and the protruding thumb, with which the biotin group interacts in the holo protein, are significantly reduced.

**Keywords:** backbone dynamics; biotin carboxyl carrier protein; nuclear magnetic resonance; post-translational modification

Post-translational modification of proteins necessary to obtain their final biological activities is found throughout nature. These include a wide range of processes such as covalent attachment by specific prosthetic groups, phosphorylation of certain amino acid residues, attachment of carbohydrate side chains, and formation of disulfide cross-links. Biotin (vitamin H or $B_8$), a small coenzyme, is attached to specific proteins through an amide linkage between its valerate side chain and the $\epsilon$-amino group of a specific lysine residue of an acceptor protein.

As a specialized carrier of one-carbon groups in their most oxidized form: $CO_2$, biotin plays a key role in many carboxylation reactions, and the biotin-dependent carboxylases constitute a class of enzymes found in organisms across the evolutionary spectrum. Four biotin-containing carboxylases are involved in the carbon chain elongation steps in mammalian metabolism: in gluconeogenesis, fatty acid synthesis, propionate metabolism, and in the catabolism of leucine. These enzymes catalyze reactions of fundamental metabolic significance involving transfer of carboxylate to a variety of substrates (Knowles, 1989). In the reaction catalyzed by the enzyme acetyl-CoA carboxylase, $CO_2$ is transferred from bicar-

Reprint requests to: Michael F. Summers, Department of Chemistry and Biochemistry, University of Maryland Baltimore County, 1000 Hilltop Circle, Baltimore, Maryland 21250; e-mail: summers@hhmi.umbc.edu.

*Abbreviations:* $\tau_e$, internal correlation times; BCCP, biotin carboxyl carrier protein; BHS, biotin holoenzyme synthetase; HOHAHA, homonuclear Hartmann–Hahn spectroscopy; HSQC, heteronuclear single quantum coherence spectroscopy; MALDI-TOFMS, matrix-assisted laser desorption/ionization–time of flight mass spectrometry; NOE, nuclear Overhauser effect; NOESY, nuclear Overhauser effect spectroscopy; $R_{ex}$, chemical exchange terms; $S^2$, generalized order parameters; $T_1$, longitudinal relaxation time constants; $T_2$, transverse relaxation time constants; TOCSY, total correlation spectroscopy.

bonate to acetyl-CoA to produce malonyl-CoA, a reaction that constitutes the first committed step in fatty acid biosynthesis. Three functional components of acetyl-CoA carboxylase participate in this two-step reaction, including the biotin carboxyl carrier, which carries the biotin moiety, biotin carboxylase, which activates $CO_2$ derived from bicarbonate by attaching it to a nitrogen in the ureido ring of biotin in an ATP-dependent reaction, and transcarboxylase, which transfers the activated $CO_2$ moiety from biotin to acetyl-CoA (Alberts & Vagelos, 1972).

Post-translational addition of biotin to a single lysine residue of apoBCCP is catalyzed by the biotin holoenzyme synthetase (BHS). The biotin ligation reaction is highly specific and in *Escherichia coli* only the BCCP subunit of acetyl-CoA carboxylase is biotinylated (Fall, 1979). In its biotinylated form, holoBCCP carries the activated $CO_2$ from the biotin carboxylase region to the active site of the transcarboxylase in the reaction in which the $CO_2$ moiety is transferred to acetyl-CoA to produce malonyl-CoA.

Structural determinants of specificity in the biotinylation of apoBCCP as well as the structural basis for interaction of holoBCCP with both the biotin carboxylase and transcarboxylase are not well understood. Greater than 76 C-terminal residues of BCCP are required for BirA-catalyzed biotinylation in vivo (Li & Cronan, 1992). Moreover, measurements of biotin carboxylase mediated carboxylation of holoBCCP are significantly faster than those measured for free biotin (G. Waldrop, pers. comm.). These results indicate that, in addition to the biotin moiety, amino acid determinants on BCCP are critical for all of the interactions in which it participates. Recently, the crystal structure of the biotinylated (or holo-) form of a carboxy-terminal domain fragment of BCCP (residue 77–156, BCCPsc) was determined at 1.8 Å resolution (Athappilly & Hendrickson, 1995), and the solution structure of the apo-form of an 87 residue C-terminal domain fragment (residue 70–156, BCCP87) of the biotin carboxyl carrier protein from *E. coli* acetyl-CoA carboxylase was solved by NMR spectroscopy techniques (Yao et al., 1997). The two structures are very similar, with small differences observed in the $\beta$ turn containing the lysine residue that is modified in the biotin ligation reaction (Athappilly & Hendrickson, 1995). It was therefore suggested that this small conformational change might be important for mediating specific interactions in which BCCP participates.

The dynamic properties of backbone $^{15}N$ spins of apoBCCP87, determined by $^{15}N$ relaxation NMR spectroscopy (Yao et al., 1997), indicate that in the absence of biotin modification there is significant conformational flexibility in the biocytin-containing loop, as well as the "protruding thumb" with which the biotin moiety is observed to interact in the crystal structure. Comparison of the dynamic data of apoBCCP87 with the crystallographic *B*-factors of holoBCCPsc suggests that the inherent mobility of these two regions is not totally lost upon biotinylation of the protein. Since the dynamic properties of proteins are correlated with local structural environment, it is of interest to determine whether the backbone dynamics of this protein are altered upon biotinylation. In this work we have utilized multidimensional NMR spectroscopy to determine the longitudinal relaxation time constants ($T_1$), the transverse relaxation time constants ($T_2$), and the steady state NOEs for the $^{15}N$ spins of holo-BCCP87 protein. Analysis of relaxation data was carried out with the model-free formalism of Lipari and Szabo (1982b). The backbone dynamic properties of holoBCCP87 indicate that upon biotinylation, the mobilities of the biocytin turn and the protruding thumb are significantly reduced. In addition, NOESY correlation peaks between the biotin group and residues within the biocytin turn and protruding thumb regions of holoBCCP87, which were found to be in good agreement with the crystal structure of holoBCCPsc, provided further evidence for small, localized conformational changes upon post-translational modification.

## Results

### *NMR spectra and assignments*

NMR studies were carried out using $^{15}N$ isotopically labeled recombinant holoBCCP87 protein samples. Signal assignments were made by analysis of two-dimensional homonuclear correlated data (Wüthrich, 1986), combined with $^{15}N$-edited two-dimensional and three-dimensional $^{15}N$-edited NOESY-HSQC, and HOHAHA-HSQC data (Marion et al., 1989a). Sequential NH-NH, NH-H$^{\alpha}$, or NH-$^{\delta}$H (for proline residues) connectivities were observed for 80 of the total 87 residues, enabling proton NMR signal assignments to be made via sequential assignment strategies (Wüthrich, 1986). The N-terminal residues Met70 to Ala76 could not be unambiguously assigned due to rapid NH exchange and to a lack of NOE signals, indicating that this segment is flexible in solution. Similar results were obtained for the apo protein (Yao et al., 1997).

As shown in the overlay of $^{1}H$–$^{15}N$ heteronuclear single quantum coherence (HSQC) spectrum of $^{15}N$-isotopically labeled holo- and apoBCCP87 (Yao et al., 1997) (Fig. 1), resonances of the majority of the $^{1}H$–$^{15}N$ correlations did not shift upon biotin binding. However, significant chemical shift changes were observed for several residues within the biocytin turn and protruding thumb (indicated by labels in Fig. 1). The backbone amide proton of Lys122, the biotinylated residue, exhibits the largest chemical shift change. In addition, its side-chain $\epsilon$-amino group, to which the biotin group is directly attached, also exhibits a $^{1}H$–$^{15}N$ cross peak, which was absent in the apo protein. A $^{1}H$–$^{15}N$ correlation peak was also observed for the backbone amide proton of Met121, which did not show a $^{1}H$–$^{15}N$ cross peak in apoBCCP87 under a similar condition (pH 7.5), due to exchange with solvent protons.

Analysis of the NMR data in terms of the apo- and holoBCCP87 structures reveals that, except for residues within the biocytin turn and the protruding thumb, the NOE cross peak patterns and intensities of the holo protein are essentially identical with those of the apo protein, indicating that the overall fold of the protein did not change upon biotinylation. Residues within the protruding thumb, which exhibited weak spin systems in apoBCCP87 due to solvent exposure and were therefore poorly defined, gave much stronger signals in data collected with the holo protein. NOE cross peaks were observed between the biotin group and residues Tyr92, Thr94, Ser96, and Pro97 as shown in Figure 2, and these NOEs are fully consistent with the crystal structure of BCCPsc (Athappilly & Hendrickson, 1995).

As previously described, the major differences between structures of apoBCCP87 and holoBCCPsc are found in the biocytin turn formed by residues Ala120–Met123 (Yao et al., 1997). The biocytin residue in BCCPsc is located at a type I′ $\beta$ turn, which is stabilized by three hydrogen bonds formed between the backbone amide protons of Ala120, Lys122, and Met123, and the carbonyl oxygens of Met123, Glu119O$\epsilon$2, and Ala120, respectively. This pattern is also observed in apoBCCP87, with the exception of the backbone amide proton of Lys122 and Glu119O$\epsilon$2 pair, which, as indicated by the NOE data, are separated by a larger distance (Yao et al., 1997). In holoBCCP87, medium intensity NOE cross peaks

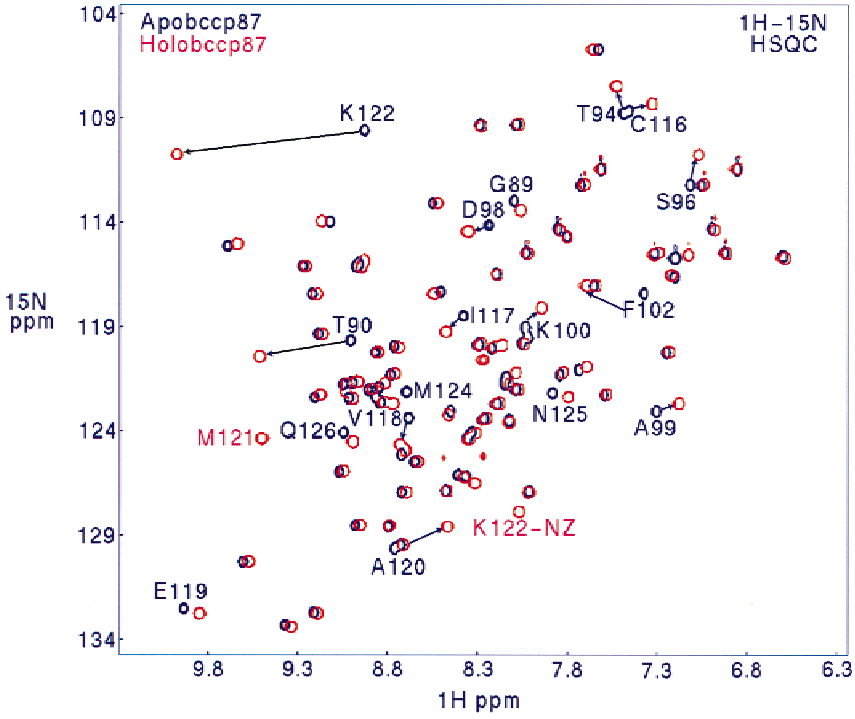


**Fig. 1.** Overlay of the two-dimensional $^{1}H$–$^{15}N$ HSQC spectra of $^{15}N$-labeled apo- and holoBCCP87 (pH 7.5, $T$ = 25.0 °C, 95% $H_2O$/5% $D_2O$). Cross peaks for the apo and the holo protein were shown in blue and red, respectively. Labels were added where significant chemical shift changes were observed between the two proteins. In addition, the backbone NH group of Met121 and the side-chain $\epsilon$-amino group of Lys122 exhibit $^{1}H$–$^{15}N$ correlation peaks (labeled in red), which were absent in the apo protein.

between backbone amide and $\alpha$-protons of Lys122 and side-chain $\gamma$-protons of Glu199 support the existence of the hydrogen bond between the backbone amide proton of Lys122 and Glu119O$\epsilon$2 atom as observed in the crystal structure. NOEs were also observed between the side-chain protons of Met124 and Ile117 and the valerate side chain and the ring protons of the biotin group. NOE cross peaks for several proton pairs within the biocytin turn, which are well within 5 Å distance in the crystal structure of holoBCCPsc (but did not give any observable NOE cross peaks in apoBCCP87), are observed in the NMR data for holoBCCP87. The only difference between the NMR data for holoBCCP87 and the X-ray structure of holoBCCPsc involves NOEs observed between the $H^{\delta}$ protons of Asn125 with the backbone amide proton and the methyl group of Ala120. These NOEs were observed in both the holo- and apoBCCP87 NMR spectra and indicate that the orientation of the side chain of Asn125 differs from that observed in the X-ray structure.

In summary, the NOEs observed for holoBCCP87 are generally consistent with the crystal structure of BCCPsc. As previously described (Yao et al., 1997), except for the residues within the biocytin turn, the solution structure of apoBCCP87 is very similar to the crystal structure of biotinylated BCCPsc. Interactions between the biotin group and the protein are localized to the biocytin turn and the protruding thumb (Athappilly & Hendrickson, 1995). We therefore conclude that biotinylation of BCCP87 protein does not impose major changes on the overall fold of the protein. However, small conformational changes localized to the biocytin turn are observed.

*Analysis of relaxation data*

The NMR relaxation parameters, including the longitudinal relaxation time constants ($T_1$), the transverse relaxation time constants ($T_2$), and the steady state $\{^{1}H\}$–$^{15}N$ NOEs, were obtained by analysis of two-dimensional proton-detected heteronuclear NMR spectroscopy, using $^{15}N$ isotopically labeled recombinant holoBCCP87 protein samples at pH 7.5. Quantitation of peak intensities from measurements of peak heights were made for 75 $^{15}NH$ backbone resonances (87 residues minus 7 unassigned residues and 5 proline residues). Uncertainties in the peak heights were estimated based on the RMS baseline noise in the spectra (Palmer et al., 1991). For comparison, $T_1$, $T_2$, and NOE values were plotted for both apo- and holoBCCP87 proteins in Figure 3. For the majority of the residues, the relaxation measurements are similar between the two proteins. Residues that exhibit significantly different $T_1$, $T_2$, or NOE values include: Thr94, Ser96, Asp98, Ala99, and Lys100 in the protruding thumb region; Glu119, Lys122, Met123, and Met124 in the biocytin turn region; and Glu150 in $\beta$8.

The "model-free" approach (Lipari & Szabo, 1982a; Lipari & Szabo, 1982b) was used to analyze the relaxation data. The procedure outlined by Mandel et al. (1995) was followed in analysis of the $T_1$, $T_2$, and NOE data. Data analysis was performed in the same manner utilized for the apo protein. The $^{15}N$ $T_1/T_2$ ratio is, to a good approximation, independent of rapid internal motions, because these motions increase the $T_1$ and $T_2$ values uniformly (Kay et al., 1989). This enables calculation of the overall rotational correlation time ($\tau_m$) from the $T_1/T_2$ ratio. However, care must be

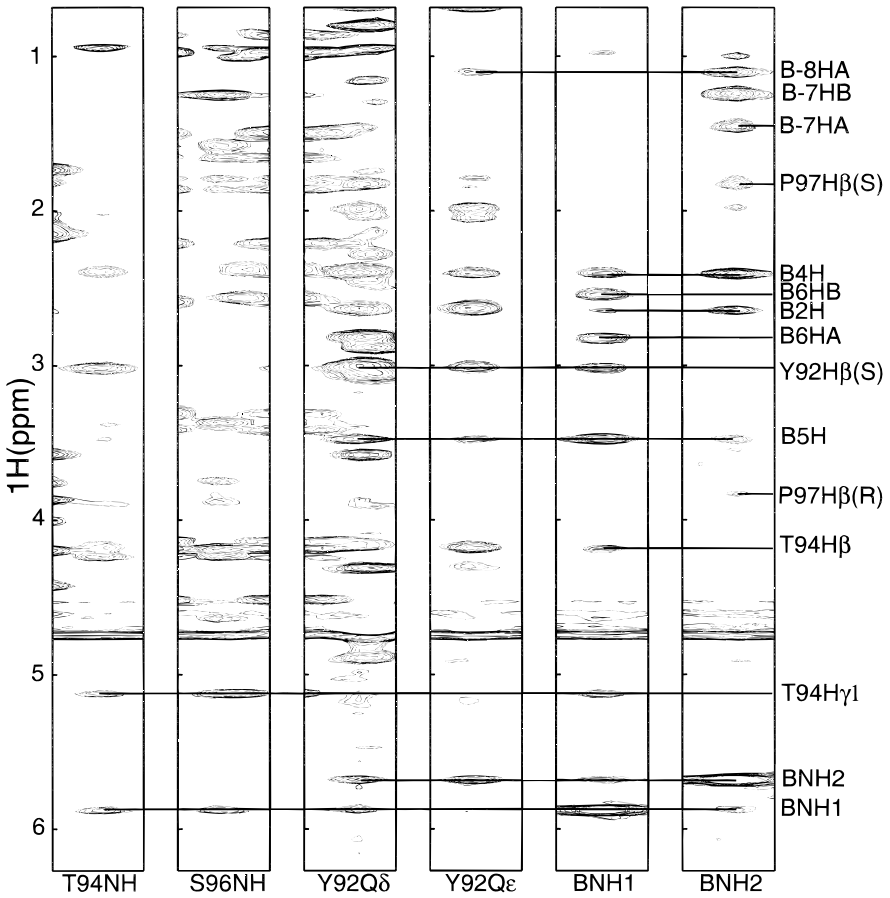


**Fig. 2.** Strips taken at the fingerprint region of the two-dimensional NOESY spectrum of holoBCCP87 showing the NOE connectivities observed between the biotin group and the protein. Strips were taken at the chemical shifts of backbone NH protons of Thr94 and Ser96, aromatic ring protons of Tyr92, and the two NH protons of the ureido group of biotin. Labels were added for NOE cross peaks of the NH protons of the ureido group with both the side-chain protons of biotin and residues Tyr92, Thr94, Ser96, and Pro97.

taken when using this method. First, residues with NOE values less than 0.6 should be excluded from such analysis. This is because the assumption that rapid internal motions do not affect the $T_1/T_2$ ratio for such residues is invalid. Consequently, the N-terminal residues Glu77, Ile78, Ser79, and Gly80 were not included in the analysis of the relaxation data. Omitting the data for these four residues, the mean values for $T_1$, $T_2$, and NOE were 0.52 ($\pm$0.03) s, 0.14 ($\pm$0.01) s, and 0.75 ($\pm$0.03) s, respectively. Second, slow conformational exchange shortens the value of $T_2$ but not of $T_1$. Therefore, a smaller than average value of $T_2$ in the absence of a concomitant increase in $T_1$ is indicative of conformational exchanges (Tjandra et al., 1996). According to this criterion, residues for which the $T_2$ value was affected by conformational exchange were excluded from the calculation, using the following relationship (Tjandra et al., 1995, 1996):

$$(\langle T_2\rangle - T_{2n})/\langle T_2\rangle - (\langle T_1\rangle - T_{1n})/\langle T_1\rangle > 1.5 \times \mathrm{SD} \qquad (1)$$

where $T_{2n}$ and $T_{1n}$ are the measured values for residue $n$, $\langle T_2\rangle$ and $\langle T_1\rangle$ are the mean values given above, and SD is the standard deviation of $(\langle T_2\rangle - T_{2n})/\langle T_2\rangle - (\langle T_1\rangle - T_{1n})/\langle T_1\rangle$. Based on this equation, residues Asp98, Ile103, Val109, Asp113, Thr134, and Glu150 were excluded from the calculation. For the remaining residues, the average value of the $T_1/T_2$ ratio, 3.76 ($\pm$0.03), was used to estimate the overall rotational correlation time $\tau_m$ = 5.27 ($\pm$0.03) ns (Palmer et al., 1991), compared to the $\tau_m$ = 5.12 ($\pm$0.03) ns of the apo protein.

Calculation of the model-free parameters from the measured relaxation data was performed using the Modelfree software (Palmer et al., 1991). Selection of optimal models for each nuclear spin was carried out using the statistical strategy outlined in Mandel et al. (1995). For each model, 500 randomly distributed synthetic data sets were generated. Dynamic models for each $^{15}$N nuclear spin were determined with the $\alpha$ = 0.5 cutoff critical value of the distribution of sum-squared error (SSE) determined from the Monte Carlo simulations (Mandel et al., 1995).

Of the 75 backbone $^{15}$N nuclear spins, relaxation data for a total of 55, 5, 11, 0, and 4 backbone $^{15}$N nuclei were fit by models 1–5, respectively—where model 1 fits only the generalized order parameter ($S^2$); model 2 fits $S^2$ and the effective internal correlation time ($\tau_e$); model 3 fits $S^2$ and the chemical exchange term ($R_{ex}$); model 4 fits $S^2$, $\tau_e$, and $R_{ex}$ terms; and model 5 fits order parameters of internal motions on both fast and slow time scales ($S_f^2$ and $S_s^2$, respectively), and also $\tau_e$. After final optimization with the

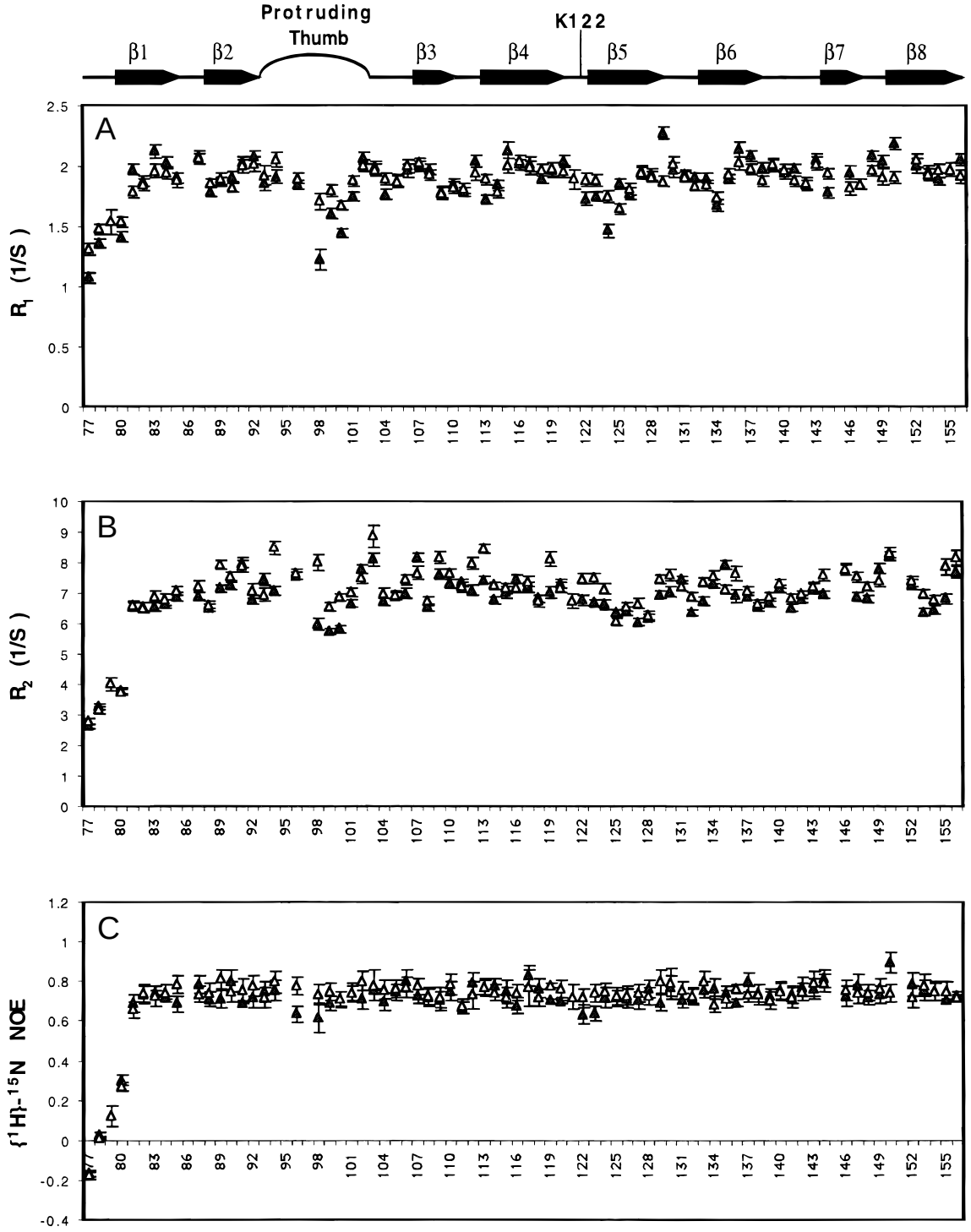


**Fig. 3.** Backbone $^{15}$N relaxation parameters for apo- and holoBCCP87. Shown are (**A**) the longitudinal relaxation time $T_1$, (**B**) the transverse relaxation time $T_2$, and (**C**) {$^1$H}–$^{15}$N NOE values plotted for the 73 residues measured of the apo protein (closed symbols, residues 77–156, excluding Ser79, Met121, and 5 proline residues), and for the 75 residues measured of the holo protein (open symbols, residues 77–156, excluding 5 proline residues). Error bars indicate the associated uncertainties in the measured values. A schematic representation of the secondary structure is shown on the top.

selected model for each nuclear spin, the global $\tau_m$ was 5.20 ns, compared to a global $\tau_m$ of 5.03 ns for the apo protein. The SSE values for 64 nuclear spins were less than the $\alpha = 0.05$ critical value; six nuclear spins had SSE values slightly greater than the critical values; six had SSE values in the range of 10–20. Excluding these latter six nuclear spins, the average values of SSE were 3.04, 0.96, and 0.00 for models with two (model 1), one (models 2 and 3), and zero (models 4 and 5) degrees of freedom, respectively.

Optimized values of the model free parameters of holoBCCP87 are presented in Table 1. The generalized order parameters $S^2$, the chemical exchange terms $R_{ex}$ for the backbone $^{15}N$ nuclear spins of both apo- and holoBCCP87, and the crystallographic *B*-factors of holoBCCPsc are plotted as a function of the residue number in Figure 4. The average value of the order parameter for all 75 measured residues in the holo protein is 0.83 (±0.13) and the values range from 0.75–0.89 for each of the eight $\beta$ stands. The average $S^2$ value for $\beta$5, 0.83 (±0.05), is slightly higher than that in the apo protein, 0.75 (±0.06). Lower than average order parameters (0.23–0.40) were observed for N-terminal residues Ile77–Gly80 in both apo- and holoBCCP87. This result is consistent with the NOE, chemical shift, and modeling data, which indicate that the N-terminal residues are disordered.

In Figure 4, residues in the protruding thumb (residues Thr94–Ala101), which also exhibit lower than average $S^2$ values, 0.73 (±0.12) in the apo protein, are significantly less mobile in the holo protein, with an average $S^2$ value is 0.85 (±0.08). Specifically, the $S^2$ value for Thr94 increases from 0.87 (±0.02) in the apo protein to 0.98 (±0.02), the highest value in the holo protein. Similarly, the $S^2$ value for Ser96 increases from 0.79 (±0.02) to 0.90 (±0.01) upon biotinylation. The increased $S^2$ values are correlated with restricted mobility on the picosecond to nanosecond time scale. This observation is in agreement with the NOESY data, which indicate a close proximity of this segment to the biotin group and the possible existence of several hydrogen bonding interactions between the two moieties. In addition, although it does not appear to be involved in the binding of biotin, the order parameter of Asp98, $S^2 = 0.52$ (±0.04), one of the lowest in the apo protein, is also significantly larger in the holo protein, 0.77 (±0.03). Slight increases in the values of $S^2$ were also observed for Ala99 and Lys100.

The biocytin turn residues (Glu119–Met124) of holoBCCP87 also exhibit higher average $S^2$ values compared with those of the apo protein. For example, the $S^2$ value for the biocytin residue Lys122 increases from 0.81 (±0.01) to 0.88 (±0.02), and the $S^2$ values for the two biotin-interacting residues Glu119 and Met124 increase from 0.86 (±0.02) to 0.93 (±0.02), and from 0.65 (±0.02) to 0.83 (±0.02), respectively. The increases in the $S^2$ values of some residues are accompanied by decreases in the conformational exchange or chemical exchange terms $R_{ex}$. For example, Met124, with a $R_{ex}$ value of 1.4 (±0.3) $S^{-1}$ in the apo protein, did not give rise to any chemical exchange term in the holo protein; similar trends were observed for residues Ser96 and Met123. These results imply that residues within the biocytin turn and the protruding thumb, especially those that are involved in the binding of the biotin moiety, exhibit both reduced internal motion on picosecond to nanosecond time scale and less extensive conformational dynamics on the chemical exchange time scale. Two additional residues, Ile127 and Ala129 of strand $\beta$5, also exhibit higher order parameters in the holo protein. The reduced internal motions of the biocytin turn in the holo protein seem to extend to the entire following $\beta$ strand.

With the exception of residues within the biocytin turn and the protruding thumb regions discussed above, residues of the holoBCCP87 protein exhibit $S^2$ values comparable to those in the apo protein. In two other cases, residues other than those in these two regions give different values in the apo and holo proteins (>0.1 different), yet no continuous stretch of residues exhibit such differences. The order parameters of holoBCCP87 correlate weakly with the crystallographic *B*-factors of holoBCCPsc, as indicated in Figure 4.

## Discussion

The solution structure of the apoBCCP87 (Yao et al., 1997) and the crystal structure of the holoBCCPsc (Athappilly & Hendrickson, 1995) were previously determined. The two structures are very similar with only small differences observed for residues in the biotin-binding turn. The NMR data presented here for holoBCCP87 are consistent with the X-ray structure, and provide further evidence for the previously proposed small, localized conformational change in the biocytin turn upon post-translational modification (Yao et al., 1997). The NMR relaxation data obtained for apo- and holo-BCCP87 reveal that the $\beta$ turn containing Lys122 and the protruding thumb exhibit rapid internal motions in the absence of the biotin group. Upon biotinylation, the mobilities of these two segments dramatically decrease and are more consistent with the mobility of the rest of the protein.

In its functional cycle, the biotin carboxyl carrier protein engages in heterologous protein–protein interactions with three distinct partners. Interaction with the biotin holoenzyme synthetase, BirA, is required for conversion of apoBCCP to the holo form protein. The biotin carboxylase subunit binds to the holoBCCP in the incorporation of the carboxylate group of bicarbonate into biotin. Finally, the carboxy-biotinylated form of BCCP interacts with transcarboxylase in the conversion of acetyl-CoA to malonyl-CoA. The data presented in this study provide evidence for a significant, localized change in the dynamic properties of the backbone $^{15}N$ spins of BCCP87, accompanied by a small, local conformational change upon protein biotinylation. These structural and dynamic changes may be significant for regulating the interaction of BCCP with the biotin carboxylase and/or the transcarboxylase.

The biotin carboxyl carrier domains of proteins from organisms ranging from bacteria to humans exhibit a high level of sequence homology (Samols et al., 1988), and cross-species biotin ligation has been demonstrated in several systems (Cronan, 1990; Leon-Del-Rio et al., 1995). Cronan (1990) demonstrated that the *E. coli* enzyme, BirA, catalyzes covalent ligation of biotin to fusion proteins containing biotin-accepting sequences derived from the 1.3 S subunit of *Propionibacterium shermanii* transcarboxylase, the *E. coli* acetyl-CoA carboxylase BCCP subunit, the $\alpha$ subunit of *Klebsiella pneumoniae* oxaloactate decarboxylase, and a protein sequence encoded by a cDNA from tomato (Cronan, 1990). This functional and sequence conservation undoubtedly reflects structural conservation, and the three-dimensional structures of both the apo- and holoBCCP protein could serve as a model for understanding the structure/function relationship of biotinyl domains in general.

However, in a recent work of the closely related biotin carboxyl carrier protein, the 1.3S subunit of *P. shermanii* transcarboxylase (Reddy et al., 1997), the similarity of the chemical shifts, relaxation parameters, and NH exchange rates of the ureido ring protons of free and 1.3S-bound biotin, as well as the absence of detectable NOE cross peaks between biotin and 1.3S, indicate that there is no strong protein–biotin interaction in the 1.3S system and little or no changes in conformation between the apo- and holo-1.3S protein. Sequence alignment of BCCPsc and 1.3S with a 30% identity suggested a similar overall fold for the two proteins. However, a seven-residue deletion of 1.3S at the equivalent position of the protruding thumb region of BCCPsc suggested the possible absence of this region in 1.3S, and the lack of interaction of 1.3S protein with biotin could be attributable to this deletion (Reddy et al., 1997). Sequence comparisons of several other biotinyl domains

**Table 1.** *Backbone $^{15}N$ model-free parameters for HoloBCCP87*

| | | | **Optimized $\tau_m$ = 5.20 ns** | | | | | | | | |
|---|---|---|---|---|---|---|---|---|---|---|---|
| Residue | 2°[a] | Model[b] | $S^2_{tot}$[c] | $dS2_{tot}$[d] | $S^2_f$ | $dS^2_f$[d] | $\tau_e$ (ps) | $d\tau_e$ (ps)[d] | $R_{ex}$ ($s^{-1}$) | $dR_{ex}$ ($s^{-1}$)[d] | *SSE*[e] |
| Glu77 | | 5 | 0.228 | 0.030 | 0.714 | 0.021 | 765 | 48 | | | |
| Ile78 | | 5 | 0.256 | 0.029 | 0.762 | 0.018 | 913 | 43 | | | |
| Ser79 | | 5 | 0.396 | 0.080 | 0.794 | 0.046 | 773 | 158 | | | |
| Gly80 | $\beta$1 | 5 | 0.342 | 0.035 | 0.747 | 0.019 | 1,075 | 77 | | | |
| His81 | $\beta$1 | 2 | 0.791 | 0.013 | | | 48 | 0.26 | | | 0.26 |
| Ile82 | $\beta$1 | 1 | 0.815 | 0.015 | | | | | | | 3.33 |
| Val83 | $\beta$1 | 2 | 0.847 | 0.017 | | | 42 | 27 | | | 1.32 |
| Arg84 | $\beta$1 | 1 | 0.855 | 0.017 | | | | | | | 4.09 |
| Ser85 | $\beta$1 | 1 | 0.858 | 0.015 | | | | | | | 0.06 |
| Pro86 | | | | | | | | | | | |
| Met87 | | 1 | 0.906 | 0.014 | | | | | | | 5.57 |
| Val88 | $\beta$2 | 2 | 0.809 | 0.013 | | | 29 | 19 | | | 1.51 |
| Gly89 | $\beta$2 | 3 | 0.859 | 0.022 | | | | | 0.84 | 0.23 | 0.16 |
| Thr90 | $\beta$2 | 3 | 0.827 | 0.021 | | | | | 0.73 | 0.26 | 0.79 |
| Phe91 | $\beta$2 | 1 | 0.931 | 0.016 | | | | | | | 2.95 |
| Tyr92 | $\beta$2 | 1 | 0.887 | 0.019 | | | | | | | 2.20 |
| Arg93 | | 1 | 0.853 | 0.020 | | | | | | | 2.21 |
| Thr94 | | 1 | 0.982 | 0.017 | | | | | | | 6.66 |
| Pro95 | | | | | | | | | | | |
| Ser96 | | 1 | 0.897 | 0.014 | | | | | | | 5.62 |
| Pro97 | | | | | | | | | | | |
| Asp98 | | 3 | 0.772 | 0.030 | | | | | 1.65 | 0.36 | 1.30 |
| Ala99 | | 1 | 0.801 | 0.013 | | | | | | | 1.47 |
| Lys100 | | 1 | 0.800 | 0.012 | | | | | | | 14.40 |
| Ala101 | | 1 | 0.851 | 0.012 | | | | | | | 1.06 |
| Phe102 | | 1 | 0.908 | 0.015 | | | | | | | 0.05 |
| Ile103 | | 3 | 0.890 | 0.023 | | | | | 1.54 | 0.42 | 0.03 |
| Glu104 | | 1 | 0.853 | 0.014 | | | | | | | 0.57 |
| Val105 | | 1 | 0.846 | 0.013 | | | | | | | 0.46 |
| Gly106 | | 1 | 0.903 | 0.016 | | | | | | | 0.18 |
| Gln107 | $\beta$3 | 1 | 0.922 | 0.015 | | | | | | | 0.40 |
| Lys108 | $\beta$3 | 1 | 0.837 | 0.013 | | | | | | | 6.19 |
| Val109 | $\beta$3 | 3 | 0.803 | 0.021 | | | | | 1.56 | 0.25 | 2.21 |
| Asn110 | $\beta$3 | 3 | 0.823 | 0.021 | | | | | 0.86 | 0.23 | 0.01 |
| Val111 | | 1 | 0.848 | 0.014 | | | | | | | 13.3 |
| Gly112 | | 1 | 0.931 | 0.017 | | | | | | | 8.73 |
| Asp113 | $\beta$4 | 3 | 0.855 | 0.018 | | | | | 1.41 | 0.21 | 0.27 |
| Thr114 | $\beta$4 | 3 | 0.806 | 0.019 | | | | | 0.61 | 0.21 | 1.52 |
| Leu115 | $\beta$4 | 1 | 0.884 | 0.017 | | | | | | | 3.24 |
| Cys116 | $\beta$4 | 1 | 0.894 | 0.014 | | | | | | | 4.98 |
| Ile117 | $\beta$4 | 1 | 0.897 | 0.017 | | | | | | | 0.09 |
| Val118 | $\beta$4 | 1 | 0.854 | 0.016 | | | | | | | 8.04 |
| Glu119 | $\beta$4 | 1 | 0.933 | 0.019 | | | | | | | 6.80 |
| Ala120 | $\beta$4 | 1 | 0.877 | 0.014 | | | | | | | 0.63 |
| Met121 | | 1 | 0.834 | 0.022 | | | | | | | 2.04 |
| Lys122 | | 1 | 0.884 | 0.016 | | | | | | | 5.24 |
| Met123 | $\beta$5 | 1 | 0.883 | 0.015 | | | | | | | 5.06 |
| Met124 | $\beta$5 | 1 | 0.830 | 0.015 | | | | | | | 7.83 |
| Asn125 | $\beta$5 | 1 | 0.740 | 0.013 | | | | | | | 2.40 |
| Gln126 | $\beta$5 | 1 | 0.807 | 0.013 | | | | | | | 2.36 |
| Ile127 | $\beta$5 | 1 | 0.836 | 0.015 | | | | | | | 6.88 |
| Glu128 | $\beta$5 | 1 | 0.807 | 0.013 | | | | | | | 16.3 |
| Ala129 | $\beta$5 | 1 | 0.882 | 0.014 | | | | | | | 5.12 |
| Asp130 | | 1 | 0.919 | 0.018 | | | | | | | 0.12 |
| Lys131 | | 1 | 0.871 | 0.014 | | | | | | | 0.86 |
| Ser132 | | 1 | 0.833 | 0.013 | | | | | | | 2.22 |
| Gly133 | $\beta$6 | 1 | 0.867 | 0.013 | | | | | | | 5.40 |
| Thr134 | $\beta$6 | 1 | 0.836 | 0.017 | | | | | | | 19.50 |
| Val135 | $\beta$6 | 1 | 0.868 | 0.014 | | | | | | | 3.64 |
| Lys136 | $\beta$6 | 1 | 0.921 | 0.019 | | | | | | | 1.58 |

(*continued*)

**Table 1.** *Continued*

| Optimized $\tau_m$ = 5.20 ns | | | | | | | | | | | |
|---|---|---|---|---|---|---|---|---|---|---|---|
| Residue | 2°[a] | Model[b] | $S^2_{tot}$[c] | $dS2_{tot}$[d] | $S^2_f$ | $dS^2_f$[d] | $\tau_e$ (ps) | $d\tau_e$ (ps)[d] | $R_{ex}$ ($s^{-1}$) | $dR_{ex}$ ($s^{-1}$)[d] | *SSE*[e] |
| Ala137 | $\beta$6 | 2 | 0.867 | 0.013 | | | 41 | 25 | | | 1.12 |
| Ile138 | $\beta$6 | 2 | 0.816 | 0.014 | | | 31 | 21 | | | 1.61 |
| Leu139 | | 1 | 0.866 | 0.014 | | | | | | | 11.2 |
| Val140 | | 1 | 0.888 | 0.013 | | | | | | | 0.94 |
| Glu141 | | 1 | 0.840 | 0.013 | | | | | | | 2.82 |
| Ser142 | | 1 | 0.844 | 0.013 | | | | | | | 0.99 |
| Gly143 | | 1 | 0.891 | 0.016 | | | | | | | 1.43 |
| Gln144 | $\beta$7 | 1 | 0.899 | 0.014 | | | | | | | 2.45 |
| Pro145 | $\beta$7 | | | | | | | | | | |
| Val146 | $\beta$7 | 3 | 0.822 | 0.022 | | | | | 1.02 | 0.26 | 0.47 |
| Glu147 | $\beta$7 | 3 | 0.837 | 0.022 | | | | | 0.65 | 0.24 | 1.17 |
| Phe148 | | 1 | 0.882 | 0.013 | | | | | | | 1.61 |
| Asp149 | | 1 | 0.887 | 0.020 | | | | | | | 1.24 |
| Glu150 | $\beta$8 | 3 | 0.863 | 0.021 | | | | | 1.22 | 0.24 | 1.55 |
| Pro151 | $\beta$8 | | | | | | | | | | |
| Leu152 | $\beta$8 | 1 | 0.911 | 0.016 | | | | | | | 2.36 |
| Val153 | $\beta$8 | 1 | 0.859 | 0.014 | | | | | | | 0.93 |
| Val154 | $\beta$8 | 1 | 0.849 | 0.015 | | | | | | | 4.88 |
| Ile155 | $\beta$8 | 1 | 0.913 | 0.020 | | | | | | | 3.17 |
| Glu156 | $\beta$8 | 1 | 0.918 | 0.019 | | | | | | | 17.9 |

[a] Secondary structures for the corresponding residues.
[b] Dynamical models selected for each nuclear spin.
[c] $S^2_{tot} = S^2_f S^2_s$ for model 5.
[d] Standard deviations for the corresponding parameters.
[e] Sum squared error values for the optimized model-free parameters.

also suggested that the protruding thumb might not exist in some of the family members of biotinyl domain proteins (Reddy et al., 1997). Therefore, while the functionality and possibly the overall folding of biotinyl domains are conserved through evolution, the detailed structures of the protein–biotin binding interface may vary in different family members.

The results of structural and dynamic studies of biotinylated domains indicate that while these proteins acquire different functionality upon biotinylation, they experience little or no structural changes. Interestingly, this is not the only case in which post-translational modification of proteins has been observed to result in moderate localized structural changes. NMR studies of both the unphosphorylated and phosphorylated forms of the phosphocarrier protein, HPr, of phosphoenolpyruvate:sugar phosphotransferase system (PTS) from *Bacillus subtilis* (Jones et al., 1997) indicate that while the overall folding of the protein is not affected by histidine phosphorylation, local conformational changes are observed at the phosphorylated His15 and residues immediately following it. Results of $T_1$ and $T_2$ measurements revealed minor changes in the dynamic properties of HPr imposed by phosphorylation. In another system in which both the oxidized and reduced forms of the disulfide reductase, thioredoxin, from *E. coli*, have been studied (Stone et al., 1993), again, structural changes are very subtle and are localized to the immediate vicinity of the active site; only several residues that are involved in the hydrophobic packing in the active site exhibit significantly different dynamic properties in the two forms of the protein. These observations suggest that the acquisition of different functionalities by proteins via post-translational modification is not necessarily accompanied by dramatic changes in their structures or dynamic properties.

## Materials and methods

### *Protein expression, purification, and characterization*

ApoBCCP87 was overexpressed from plasmid pTM53 in *E. coli* strain BL21$\lambda$DE3 (provided by Dr. John Cronan, Jr.) and purified as described previously (Nenortas & Beckett, 1996). $^{15}$N labeling of apoBCCP87 was achieved as described previously (Yao et al., 1997).

HoloBCCP87 was derived from apoBCCP87 enzymatically by BirA-catalyzed biotin ligation. The reaction contained 200 $\mu$M apoBCCP87, 300 $\mu$M bio-5′-AMP (in excess), 1 $\mu$M BirA in 10 mL of buffer containing 10 mM Tris·HCl, 200 mM KCl, and 2.5 mM $MgCl_2$, pH 7.5 at 20 °C, and was allowed to proceed for 1 h. The reaction mixture was then dialyzed against 20 mM potassium phosphate at pH 7.0, 5% glycerol at 4 °C. The sample was loaded onto a DEAE-sephacel column equilibrated in the same buffer, and holoBCCP87 was eluted using a linear 20–200 mM potassium phosphate gradient. Quantitative incorporation of the biotin group into BCCP87 was confirmed by MALDI-TOFMS as previously described (Nenortas & Beckett, 1996).

### *Nuclear magnetic resonance spectroscopy*

HoloBCCP87 samples (1.0–2.0 mM) for NMR were prepared in either 95% $H_2O$/5% $D_2O$ or $D_2O$, containing 100 mM KCl, 2.5 mM $MgCl_2$, and 10 mM phosphate buffer (pH 7.5), identical to the buffer conditions used for the apo protein (Yao et al., 1997). NMR data were collected with General Electric Omega PSG ($^1$H) and Bruker DMX 600 MHz ($^1$H) spectrometers with the sample

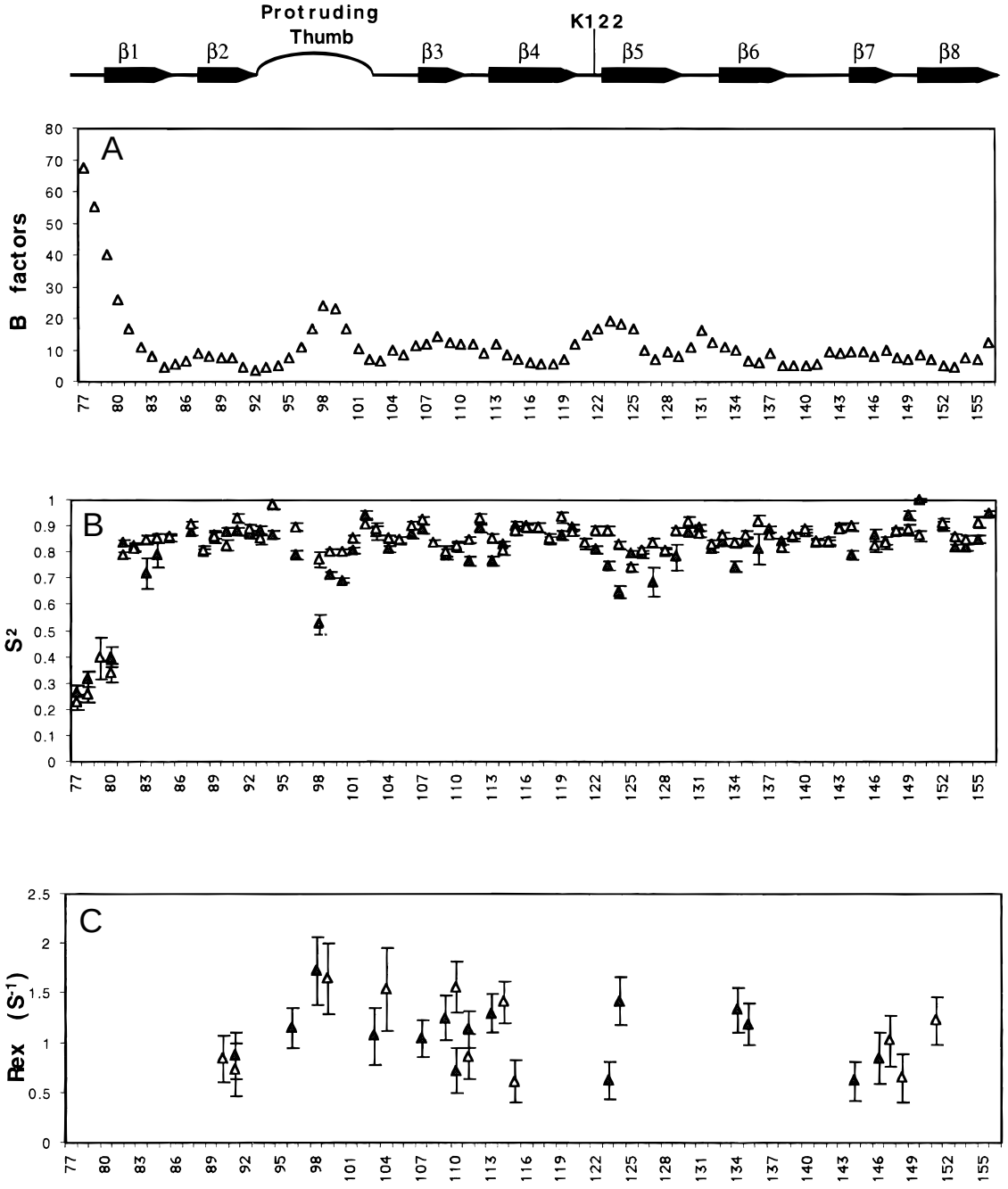


**Fig. 4.** Comparison of the X-ray crystallographic *B*-factors of holoBCCPsc with the model-free parameters of backbone $^{15}N$ spins of apo- and holoBCCP87. **A**: The *B*-factors of holoBCCPsc (open symbols). **B**: The generalized order parameters $S^2$ of apoBCCP87 (closed symbols) and holoBCCP87 (open symbols). **C**: The chemical exchange term $R_{ex}$ of apoBCCP87 (closed symbols) and holoBCCP87 (open symbols). Error bars indicate the associated uncertainties in the calculated values. The diagram on the top is a schematic representation of the secondary structure.

maintained at 25 °C. Two-dimensional NOESY data were collected with 150 ms mixing time without presaturation. Two-dimensional homonuclear Hartmann–Hahn (HOHAHA) spectra were collected using a 76 ms MLEV-17 spin-lock duration. In both experiments, water suppression was achieved using WATERGATE read pulses prior to acquisition (Piotto et al., 1992). 2QF-COSY spectra were collected with a continuous wave solvent presaturation followed by a Scuba pulse train of 40 ms. All of these two-dimensional experiments were also collected with samples in $D_2O$ without water suppression. For some experiments, the initial sampling delay was set to one-half the $t_1$ dwell period to eliminate baseline distortions in the $F1$ dimension (Marion & Bax, 1989; Marion et al., 1989c). In many cases, alternate-block acquisition mode was utilized to minimize $t_1$ noise.

Two-dimensional $^1H$–$^{15}N$ HSQC (Bax et al., 1990) and three-dimensional $^{15}N$-edited NOESY-HSQC (Marion et al., 1989a),

$^{15}N$, $^{15}N$-edited HMQC-NOESY-HSQC (Ikura et al., 1990), and $^{15}N$-edited HNHB data were acquired with the uniformly $^{15}N$-labeled holoBCCP87 sample (95% $H_2O$/5% $D_2O$), using water flip-back (Grzesiek & Bax, 1993) and field gradient pulses (Piotto et al., 1992) to suppress the water signal without saturation. The initial $^{15}N$ evolution period ($F2$) were set to one-half the dwell to remove baseline distortions (Bax et al., 1991; Zhu et al., 1993). A mixing time of 150 ms was used for all NOESY data. Three-dimensional $^{15}N$-edited TOCSY-HSQC (Marion et al., 1989a) data were obtained with a 70 ms clean-MLEV-17 spin lock duration (Griesinger et al., 1988) and sensitivity-improved gradient coherence selection (Zhang et al., 1994). WALTZ-16 (Shaka et al., 1983) modulation was used in all $^{15}N$-edited experiments to decouple $^{15}N$ during acquisition. For all measurements $^1H$ carrier was set to the water resonance (4.773 ppm at 25 °C) with 9,090 Hz spectral width and 112 ms acquisition time. The $^{15}N$ carrier was set to 118 ppm with 1,642 Hz spectral width.

Two-dimensional proton-detected heteronuclear NMR spectroscopy was used to measure longitudinal relaxation rate constants ($R_1$), transverse relaxation rate constants ($R_2$), and $\{^1H\}$-$^{15}N$ steady-state heteronuclear Overhauser effects (NOE) for the backbone $^{15}N$ spins of uniformly $^{15}N$-labeled holoBCCP87, under experimental conditions similar to those utilized for apoBCCP87 (Yao et al., 1997). Relaxation measurements were performed using inversion recovery (Vold et al., 1968), Carr-Purcell-Meiboom-Gill (CPMG) (Carr & Purcell, 1954; Meiboom & Gill, 1958), and steady-state NOE (Noggle & Shirmer, 1971) pulse sequences previously described (Barbato et al., 1992; Kay et al., 1992; Peng & Wagner, 1992; Farrow et al., 1994). Dipolar relaxation and chemical-shift anisotropy cross correlation were removed by proton 180° pulses applied every 5–10 ms during the relaxation delay. The $t_1$ evolution is designed as a semi-constant time period to optimize the acquired signal in the $t_1$ dimension. Decoupling during acquisition was performed using WALTZ16 (Shaka et al., 1983). $T_1$ and $T_2$ were collected with 1.5 s pre-delay. $T_1$ data were collected at 30, 120, 250, 380, 510, 630, 760, and 1,020 ms. $T_2$ data were collected at 8, 40, 88, 136, 184, 248, 312, and 376 ms. The $\{^1H\}$–$^{15}N$ steady-state NOE values were obtained by recording spectra with and without the use of proton saturation before the start of the experiment. Proton saturation was applied for 3 s, and 3 s pre-delay was used for the NOE spectra; the reference spectrum was recorded with 6 s pre-delay without saturation. Data were collected with the water flip-back pulses (Grzesiek & Bax, 1993) and WATERGATE read pulses to achieve water saturation (Piotto et al., 1992). $T_1$ and $T_2$ data were collected with 16 scans and NOE data were collected with 32 scans per $t_1$ points. All data sets were collected twice with $^1H$ carrier set to the water resonance with 9,090 Hz spectral width and 112 ms acquisition time. The $^{15}N$ carrier was set to 118 ppm with 1,642 Hz spectral width and 256 complex points were collected starting at one-half dwell time with States_TPPI for quadrature detection (Marion et al., 1989b; Bax et al., 1991).

NMR spectra were processed with NMRPipe software (Delaglio et al., 1995). The two-dimensional NOESY, TOCSY, and COSY were processed using 70°-shifted squared sine bell filtering in $t_2$ and 60°-shifted squared sine bell in $t_1$. The two-dimensional $^1H$–$^{15}N$ HSQC spectra were processed using 90°-shifted squared sine bell in both $t_1$ and $t_2$. Three-dimensional $^{15}N$-edited NOESY-HSQC and $^{15}N$-edited TOCSY were processed using 60°-shifted squared sine bell in $t_3$. Three-dimensional $^{15}N$-edited NOESY-HSQC data were doubled by mirror-image linear prediction in $t_2$ ($^{15}N$), and apodized in $t_1$ ($^1H$) and $t_2$ by 60°- and 70°-shifted squared sine bell, respectively, with zero filling to 512 and 128 real data points, respectively. Three-dimensional $^{15}N$-edited TOCSY data were linear predicted in $t_1$ ($^{15}N$) and $t_2$ ($^1H$) to 64 and 192, respectively, and apodized by 75°-shifted squared sine bell, with zero filling to 128 and 512, respectively. Three-dimensional $^{15}N$-edited HNHB data were mirror image linear predicted in $t_1$ ($^{15}N$) and linear predicted in $t_2$ ($^1H$), respectively, and apodized by 90°- and 80°-shifted squared sine bell with zero filling to 128 and 256 complex points, respectively. $T_1$, $T_2$, and NOE spectra were processed with 70°-shifted squared sine bell in both dimensions and zero filled to 512 in $t_1$ ($^{15}N$) dimension.

All data analysis was done with NMRVIEW software (Johnson & Blevins, 1994). For $T_1$ and $T_2$ dynamics measurements, cross-peak intensities were measured from peak heights and fit to an exponential decay function by nonlinear least-squares analysis using the Levenburg–Marquadt method (Press et al., 1992). NOE values were determined as the ratios of the peak intensities measured from spectra acquired with and without proton saturation during the recycle delay.

## Acknowledgments

This work was supported by NIH grant GM 46511 (D.B.). We are grateful to Dr. M. Zawrotny and R. Edwards (UMBC, Howard Hughes Medical Institute) for technical support.

## References

Alberts AW, Vagelos PR. 1972. Acyl-CoA carboxylases. In: Boyer PD, ed. *The enzymes*, Vol 6. pp 37–82. Ed. 3. New York: Academic Press.

Athappilly FK, Hendrickson WA. 1995. Structure of the biotinyl domain of acetyl-coenzyme A carboxylase determined by MAD phasing. *Structure 3*:1407–1419.

Barbato G, Ikura M, Kay LE, Pastor RW, Bax A. 1992. Backbone dynamics of calmodulin studied by $^{15}N$ relaxation using inverse detected two-dimensional NMR spectroscopy: The central helix is flexible. *Biochemistry 31*:5269–5278.

Bax A, Ikura M, Kay LE, Torchia DA, Tschudin R. 1990. Comparison of different modes of two-dimensional reverse correlation NMR for the study of proteins. *J Magn Reson 86*:304–318.

Bax A, Ikura M, Kay LE, Zhu G. 1991. Removal of F1 baseline distortion and optimization of folding in multidimensional NMR spectra. *J Magn Reson 91*:174–178.

Carr HY, Purcell EM. 1954. Effects of diffusion on free precession in nuclear magnetic resonance experiments. *Phys Rev 4*:630–638.

Cronan JE Jr. 1990. Biotination of proteins in vivo. *J Biol Chem 265*: 10327–10333.

Delaglio F, Grzesiek S, Vuister GW, Zhu G, Pfeifer J, Bax A. 1995. NMRPipe: A multidimensional spectral processing system based on UNIX pipes. *J Biomol NMR 6*:277–293.

Fall RR. 1979. Analysis of microbial biotin proteins. *Methods Enzymol 62*:390–398.

Farrow NA, Muhandiram R, Singer AU, Pascal SM, Kay CM, Gish G, Shoelson SE, Pawson T, Forman-Kay JD, Kay LE. 1994. Backbone dynamics of a free and a phosphopeptide-complexed Src homology 2 domain studied by $^{15}N$ NMR relaxation. *Biochemistry 33*:5984–6003.

Griesinger C, Otting G, Wüthrich K, Ernst RR. 1988. Clean TOCSY for $^1H$ spin system identification in macromolecules. *J Am Chem Soc 110*:7870–7872.

Grzesiek S, Bax A. 1993. The importance of not saturating $H_2O$ in protein NMR—Application to sensitivity enhancement and NOE measurement. *J Am Chem Soc 115*:12593–12593.

Ikura M, Bax A, Clore GM, Gronenborn AM. 1990. Detection of nuclear Overhauser effects between degenerate amide proton resonances by heteronuclear three-dimensional nuclear magnetic resonance spectroscopy. *J Am Chem Soc 112*:9020–9022.

Johnson BA, Blevins RA. 1994. NMR view: A computer program for the visualization and analysis for NMR data. *J Biomol NMR 4*:603–614.

Jones BE, Rajagopal P, Klevit RE. 1997. Phosphorylation on histidine is ac-

companied by localized structural changes in the phosphocarrier protein HPr from *Bacillus subtilis*. *Protein Sci 6*:2107–2119.

Kay LE, Nicholson LK, Delaglio F, Bax A, Torchia DA. 1992. Pulse sequences for the removal of the effects of cross correlation between dipolar and chemical shift anisotropy relaxation mechanisms on the measurement of heteronuclear $T_1$ and $T_2$ values in proteins. *J Magn Reson 97*:359–375.

Kay LE, Torchia DA, Bax A. 1989. Backbone dynamics of proteins as studied by $^{15}$N inverse detected heteronuclear NMR spectroscopy: Application to staphylococcal nuclease. *Biochemistry 28*:8972–8979.

Knowles JR. 1989. The mechanism of biotin-dependent enzymes. *Ann Rev Biochem 58*:195–221.

Leon-Del-Rio A, Leclerc D, Akerman B, Wakamatsu N, Gravel RA. 1995. Isolation of a cDNA encoding human holocarboxylase synthetase by functional complementation of a biotin auxotroph of *Escherichia coli*. *Proc Natl Acad Sci USA 92*:4226–4230.

Li S-J, Cronan JE Jr. 1992. The gene encoding the biotin carboxylase subunit of *Escherichia coli* acetyl-CoA carboxylase. *J Biol Chem 267*:855–863.

Lipari G, Szabo A. 1982a. Model-free approach to the interpretation of nuclear magnetic resonance relaxation in macromolecules. 1. Theory and range of validity. *J Am Chem Soc 104*:4546–4559.

Lipari G, Szabo A. 1982b. Model-free approach to the interpretation of nuclear magnetic resonance relaxation in macromolecules. 2. Analysis of experimental results. *J Am Chem Soc 104*:4559–4570.

Mandel AM, Mikael A, Palmer AG. 1995. Backbone dynamics of *Escherichia coli* Ribonuclease HI: Correlations with structure and function in an active enzyme. *J Mol Biol 246*:144–163.

Marion D, Bax A. 1989. Baseline correction of 2D FT NMR spectra using a simple linear prediction extrapolation of the time-domain data. *J Magn Reson 83*:205–211.

Marion D, Driscoll PC, Kay LE, Wingfield PT, Bax A, Gronenborn AM, Clore GM. 1989a. Overcoming the overlap problem in the assignment of $^1$H NMR spectra of larger proteins by use of three-dimensional heteronuclear $^1$H-$^{15}$N Hartmann-Hahn-multiple quantum coherence and nuclear Overhauser-multiple quantum coherence spectroscopy: Application to interleukin 1$\beta$. *Biochemistry 28*:6150–6156.

Marion D, Ikura M, Tschudin R, Bax A. 1989b. Rapid recording of 2D NMR spectra without phase cycling. Application to the study of hydrogen exchange in proteins. *J Magn Reson 85*:393–399.

Marion D, Kay LE, Sparks SW, Torchia DA, Bax A. 1989c. Three-dimensional heteronuclear NMR of $^{15}$N-labeled proteins. *J Am Chem Soc 111*:1515–1517.

Meiboom S, Gill D. 1958. Modified spin-echo method for measuring nuclear spin relaxation times. *Rev Sci Instrum 29*:688–691.

Nenortas E, Beckett D. 1996. Purification and characterization of intact and truncated forms of the *Escherichia coli* biotin carboxyl carrier subunit of acetyl-CoA carboxylase. *J Biol Chem 271*:7559–7567.

Noggle JH, Shirmer RE. 1971. *The nuclear Overhauser effect: Chemical applications*. New York: Academic Press. pp 1–259.

Palmer AG, Rance M, Wright PE. 1991. Intramolecular motions of a zinc finger DNA-binding domain from xfin characterized by proton-detected natural abundance $_{13}$C heteronuclear NMR spectroscopy. *J Am Chem Soc 113*:4371–4380.

Peng JW, Wagner G. 1992. Mapping of spectral density functions using heteronuclear NMR relaxation measurements. *J Magn Reson 98*:308–332.

Piotto M, Saudek V, Sklenar V. 1992. Gradient tailored excitation for single quantum NMR spectroscopy of aqueous solutions. *J Biomol NMR 2*:661–665.

Press WH, Teukolsky SA, Vetterling WT, Flannery BP. 1992. *Numerical recipes in C: The art of scientific computing*, 2nd ed. Cambridge, United Kingdom: Cambridge University Press.

Reddy DV, Shenoy BC, Carey PR, Sönnichsen FD. 1997. Absence of observable biotin-protein interactions in the 1.3S subunit of transcarboxylase: An NMR study. *Biochemistry 36*:14676–14682.

Samols D, Thornton CG, Murtif VL, Kumar GK. 1988. Evolutionary conservation among biotin enzymes. *J Biol Chem 263*:6461–6464.

Shaka AJ, Keler J, Freeman R. 1983. Evaluation of a new broadband decoupling sequence: WALTZ-16. *J Magn Reson 53*:313–340.

Stone MJ, Chandrasekhar K, Holmgren A, Wright PE, Dyson HJ. 1993. Comparison of backcone and tryptophan side-chain dynamics of reduced and oxidized *Escherichia coli* thioredoxin using $^{15}$N NMR relaxation measurements. *Biochemistry 32*:426–435.

Tjandra N, Feller SE, Pastor RW, Bax A. 1995. Rotational diffusion anisotropy of human ubiquitin from $^{15}$N NMR relaxation. *J Am Chem Soc 117*:12562–12566.

Tjandra N, Wingfield P, Stahl S, Bax A. 1996. Anisotropic rotational diffusion of perdeuterated HIV protease from $^{15}$N NMR relaxation measurements at two magnetic fields. *J Biomol NMR 8*:273–284.

Vold RL, Waugh JS, Klein MP, Phelps DE. 1968. Measurement of spin relaxation in complex systems. *J Chem Phys 48*:3831–3832.

Wüthrich K. 1986. *NMR of proteins and nucleic acids*. New York: John Wiley & Sons.

Yao X, Wei D, Soden JC, Summers MF, Beckett D. 1997. Structure of the carboxy-terminal fragment of the apo-biotin carboxyl carrier subunit of *Escherichia coli* acetyl-CoA carboxylase. *Biochemistry 36*:15089–15100.

Zhang O, Kay LE, Olivier JP, Forman-Kay JD. 1994. Backbone $_1$H and $_{15}$N resonance assignments of the N-terminal SH3 domain of drk in folded and unfolded states using enhanced sensitivity pulsed field gradient NMR techniques. *J Biomol NMR 4*:845–858.

Zhu G, Torchia DA, Bax A. 1993. Discrete Fourier transformation of NMR signals. The relationship between sampling delay time and spectral baseline. *J Magn Reson A 105*:219–222.